SIAM J. APPL. MATH.
Vol. 80, No. 2, pp. 690–705

ELASTIC FINGERING OF A BONDED SOFT DISC IN TRACTION: INTERPLAY OF GEOMETRIC AND PHYSICAL NONLINEARITIES*

PASQUALE CIARLETTA†, HUI-HUI DAI‡, AND MATTEO TAFFETANI§

Abstract. This work provides a mathematical understanding of the elastic fingering provoked by a large axial extension of a soft solid cylinder bonded between rigid plates. In this prototypical system model, a topological transition from a ground axis-symmetric meniscus is quasi-statically controlled by the applied displacement, which acts as the order parameter of a pitchfork bifurcation. Since the isotropic elastic energy becomes nonconvex under finite strains, geometric nonlinearity is of paramount importance for the loss of uniqueness of the solution of the boundary value problem. Nonetheless, physical nonlinearity in the elastic energy is found to exert an opposite stabilizing effect. It indeed penalizes the local stretching at the free boundary that would arise as a consequence of any change of its Gaussian curvature. The theoretical and numerical results are in agreement with recent experimental observations, showing that elastic fingering is strongly affected by the aspect ratio of the disc and can be even suppressed in soft materials with physical nonlinearity.

Key words. bifurcation theory, solid mechanics, finite elasticity, elastic stability

AMS subject classifications. 74B20, 74G60, 74H15

DOI. 10.1137/19M1289297

1. Introduction.

A dynamic patterning is commonly observed at the interface between viscous fluids, causing the onset and the evolution of fingers of the displacing fluid into the displaced one [29, 28, 20]. This fluid mechanical instability received extensive mathematical attention due to its fundamental importance in many industrial processes, such as oil drilling [15]. The problem canonically translates into a nonlinear moving-boundary problem for elliptic equations, which can be solved using complex variable techniques in simplified geometries [24, 4], sharing similarities with pattern formation mechanisms in different nonequilibrium systems, e.g., dendritic growth [3] and failure of adhesive bonding [11, 2].

Bulk fingering has been recently observed also at solid-solid interfaces, for example, when pumping air into a geometrically constrained elastomer [30] or pulling an adherent elastic meniscus [31, 5]. While viscous fingering is a dynamically unstable process, bulk fingering in soft solids has an intrinsically different physical origin, occurring as a marginally stable state after an elastic bifurcation. In this work, we focus on the elastic fingering provoked by a large axial extension of a soft solid cylinder bonded to rigid plates at its planar ends. In this prototypical system model, the topological transition from a ground axis-symmetric state is quasi-statically controlled by the applied displacement at the rigid ends, which acts as the order parameter of the elastic bifurcation. Since the elastic energy becomes nonconvex under finite displacements, geometric nonlinearities are of paramount importance for the loss of uniqueness of the

*Received by the editors September 27, 2019; accepted for publication (in revised form) January 6, 2020; published electronically March 3, 2020.
https://doi.org/10.1137/19M1289297
Funding: This work was supported by MIUR, PRIN 2017 Research Project "Mathematics of active materials: From mechanobiology to smart devices."
†MOX, Politecnico di Milano, Milan, Italy (pasquale.ciarletta@polimi.it).
‡Department of Mathematics, City University of Hong Kong, Hong Kong (mahhdai@cityu.edu.hk).
§Mathematical Institute, University of Oxford, Oxford OX2 6GG, UK (matteo.taffetani@maths.ox.ac.uk).

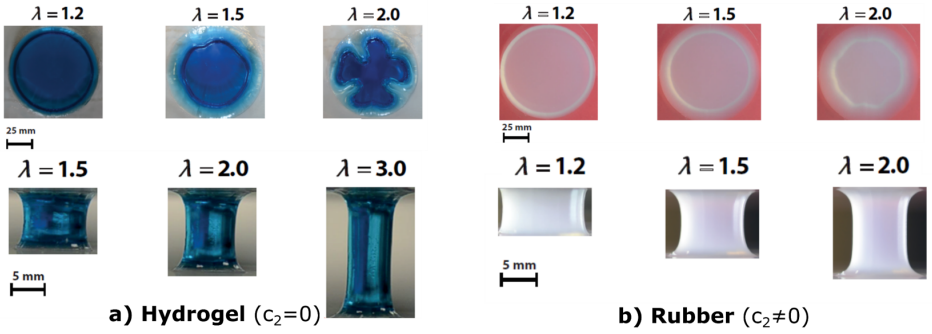

FIG. 1. *Traction load experiments on discs made of a hydrogel (left, $c_2 = 0$, $L/R_0 = 1/6$ (top), $L/R_0 = 1/2$ (bottom)) and a rubber-like material (right, $c_2 \neq 0$, $L/R_0 = 1/2$). The hydrogel disc displays fingering at a critical stretch threshold, while the rubber disc keeps an axis-symmetric shape. Adapted with permission from* [19].

elastic boundary value problem [13]. The marginal thresholds and the morphology of elastic fingers have been experimentally characterized using hydrogels [18], showing that they are greatly affected by the initial shape of the body. Nonetheless, elastic fingering may be suppressed in different soft materials, such as rubbers [19], as illustrated in Figure 1. These experimental results lack any theoretical explanation, suggesting that the physical nonlinearities in the specific strain-stiffening response of the material may counterbalance the geometric effects. The aim of this work is to provide a mathematical understanding of the interplay between the geometric and the physical nonlinearities on the onset and the full development of fingering for an isotropic, incompressible, nonlinear elastic material.

The article is organized as follows. In section 2, we formulate the constitutive assumptions and the corresponding nonlinear elastic boundary value problem. We give in section 3 its axis-symmetric solution that is used as the ground state. In section 4, we perform the linear bifurcation analysis of this ground state using the incremental method of small deformations superposed on finite strains. We derive a generalized Stroh formulation of the incremental problem, which is solved analytically for the neo-Hookean and extreme Mooney models. A numerical procedure is also introduced to solve the incremental problem in the general case. The results of the linear stability analysis are collected in section 5, together with the numerical simulations of the fully developed fingering using a mixed finite element formulation of the discrete problem. Finally, section 6 contains a discussion of the results and a few concluding remarks.

2. The nonlinear elastic model. Let us consider a homogeneous solid cylinder in the three-dimensional Euclidean space $\mathbb{E}^3$, where (r, θ, z) and (R, Θ, Z) are the polar cylindrical coordinates in its current and reference configurations, respectively, with $\mathbf{x}$ and $\mathbf{X}$ being the spatial and material position vectors. The cylinder has initial length $2L$ and radius R_0, so that the reference domain is

$$\Omega_0 = \left\{ \mathbf{X} \in \mathbb{E}^3 : 0 \leq R < R_0, \quad 0 \leq \theta < 2\pi, \quad -L < Z < L \right\}.$$

The dimensionless parameter R_0/L will be referred to in the following as the initial aspect ratio of the body, being the inverse of slenderness ratio. We assume that the mapping $\mathbf{x} = \mathbf{x}(R, \Theta, Z)$ is twice continuously differentiable, so that the geometrical deformation tensor is given by $\mathsf{F} = \mathrm{Grad}\mathbf{x} = \frac{\partial \mathbf{x}}{\partial \mathbf{X}}$, with $\mathsf{B} = \mathsf{F}\mathsf{F}^T$ being the left Cauchy–Green tensor. The cylinder is made of a homogeneous, incompressible, nonlinear

elastic material, and its elastic strain energy density $W = W(\mathsf{F})$ if taken of the Mooney–Rivlin form [21, 27]:

$$W(\mathsf{F}) = \psi(\mathsf{F}) - p(\det \mathsf{F} - 1) \qquad \text{with} \quad \psi(\mathsf{F}) = c_1(I_1 - 3) + c_2(I_2 - 3), \tag{2.1}$$

where $I_1 = \mathrm{tr}\mathsf{B}$, $I_2 = 1/2\left((\mathrm{tr}\mathsf{B})^2 - \mathrm{tr}(\mathsf{B}^2)\right)$ and p is the Lagrangian multiplier enforcing the internal constraint of incompressibility. The shear modulus of the material is $\mu = 2c_1 + 2c_2 > 0$, and the ratio $c_2/c_1 \geq 0$ will be taken as the characteristic dimensionless parameter for the constitutive response. In particular, c_2/c_1 represents the effect of physical nonlinearity of the constitutive law, since the lower neo-Hookean limit $c_2 = 0$ only contains geometrical nonlinearity, and the upper limit $c_1 = 0$ is the extreme Mooney material.

From (2.1), the nominal stress tensor P reads

$$\mathsf{P} = 2c_1\mathsf{F}^T - 2c_2\mathsf{F}^{-1}\mathsf{B}^{-1} + (2c_2 I_2 - p)\mathsf{F}^{-1}. \tag{2.2}$$

Neglecting body forces, the equilibrium equations impose $\mathsf{FP} = \mathsf{P}^T\mathsf{F}^T$ and

$$\mathrm{Div}\mathsf{P} = \mathbf{0}, \tag{2.3}$$

where Div is the material divergence operator [35]. Finally, the cylinder is bonded between two rigid end plates at the Dirichlet boundary $\partial\Omega_D = \{\mathbf{X} \in \mathbb{E}^3 : Z = \pm L\}$, so that

$$z(Z = \pm L) = \pm\lambda L, \qquad r(Z = \pm L) = R, \qquad \theta(Z = \pm L) = \Theta, \tag{2.4}$$

so that the overall axial stretch $\lambda \geq 1$ is sustained by tensile traction loads at the end plates, while the disc is free of external tractions at the outer Neumann boundary $\partial\Omega_N = \{\mathbf{X} \in \mathbb{E}^3 : R = R_0\}$.

3. Analysis of the axis-symmetric solution. The axis-symmetric solution for a bonded circular disc was first analyzed by Klingbeil and Shield [16]. In the following, we retrace the main steps for deriving the physical fields in the traction case $\lambda > 1$, reporting their analytic expression for the limiting case of neo-Hookean and extreme Mooney materials, and the semianalytic solution for a Mooney–Rivlin body.

Assuming axial symmetry, we set

$$r = r(R, Z), \quad \theta = \Theta, \quad z = z(R, Z),$$

so that r is an even function of Z, with $r(R = 0) = 0$, and z is an odd function of Z. Such an axis-symmetric solution can be found under the simplifying assumption that the planes initially at constant Z remain plane in the deformed state, so that

$$z = g(Z), \qquad r = R\ f(Z), \tag{3.1}$$

so that the deformation gradient reads

$$\mathsf{F} = \begin{bmatrix} f & 0 & R\ f' \\ 0 & f & 0 \\ 0 & 0 & g' \end{bmatrix},$$

where prime denotes differentiation. The incompressibility constraint $\det \mathsf{F} = 1$ imposes

$$g' = f^{-2}.$$

The axis-symmetric Lagrange multiplier $p = p(R, Z)$ can be derived by the equilibrium equation (2.3) using (2.2), such that

$$\begin{cases} \frac{\partial p}{\partial R} = 2c_1 R f\ f'' + 2c_2 R f^2 (f\ f'' + f'^2); \\ \frac{\partial p}{\partial Z} = 2c_1 (R^2 f\ f'' - 2f'/f^5) + 2c_2 (R^2 f f' (f\ f'' + f'^2) - 2f'/f^3). \end{cases} \tag{3.2}$$

Combining the two previous equations one finds a differential equation for f, being

$$c_1 \frac{f''}{f} + c_2 \frac{(f^2)''}{2} = (c_1 + c_2) A^2, \tag{3.3}$$

where A is a constant of integration that will be fixed by the boundary conditions (2.4) on $\partial\Omega_D$, that impose

$$f'(0) = 0, \quad f(L) = 1, \quad g(L) = \lambda\ L. \tag{3.4}$$

The general solution of (3.3) and (3.4) can be expressed in the form of an elliptic function and an elliptic integral; while analytic solutions will be summarized later for the neo-Hookean and the extreme Mooney case. From (3.2), (3.3), the field p takes the following expression:

$$p = \left(\mu B + \frac{1}{2} (A\ R\ f)^2 + c_1 \frac{1}{f^4} \right) + c_2 \frac{2}{f^2}, \tag{3.5}$$

where B is a further constant of integration that will be fixed by the boundary conditions on $\partial\Omega_N$. The determination of B requires a further assumption, because the stress component P_{RR} cannot vanish everywhere at $\partial\Omega_N$. Since $Z = 0$ is a plane of symmetry for the deformation, in the limit of thick cylinders, i.e., $L/R_0 \ll 1$, we can impose at the leading order that $P_{RR}(R_0, 0) = 0$, so that

$$B = \frac{f(0)^6 ((A^2 - 2)c_1 + A^2 c_2) + c_1 - 2c_2 f(0)^8}{2(c_1 + c_2) f(0)^4}. \tag{3.6}$$

We remark that the same simplification was proposed in [18] from a different energy minimization standpoint, while it is here derived from a lubrication limit as in [6]. Figure 2 (left) depicts the deformed shape of an elastic cylinder with $R_0 = 10\ L$ at different levels of applied stretch λ for $c_1 = c_2$, showing the formation of a characteristic meniscus at $\partial\Omega_N$. We compare in Figure 2 (right) the shapes of the meniscus at different values of the ratio c_2/c_1 at fixed applied stretch $\lambda = 1.5$, computed by numerical integration using the Runge–Kutta method. In particular, we remark that the meniscus becomes deeper as c_2/c_1 increases.

Finally, we collect in the next subsections the analytic solution for the neo-Hookean and extreme-Mooney materials for future convenience.

3.1. Analytic solution for the neo-Hookean model ($c_2 = 0$). Equation (3.3) can be integrated explicitly for a neo-Hookean strain energy density, such that

$$f = \frac{\cosh(AZ)}{\cosh(AL)}; \qquad g = \lambda L \frac{\tanh(AZ)}{\tanh(AL)} \tag{3.7}$$

with

$$\lambda = \frac{\sinh(2AL)}{2AL}. \tag{3.8}$$

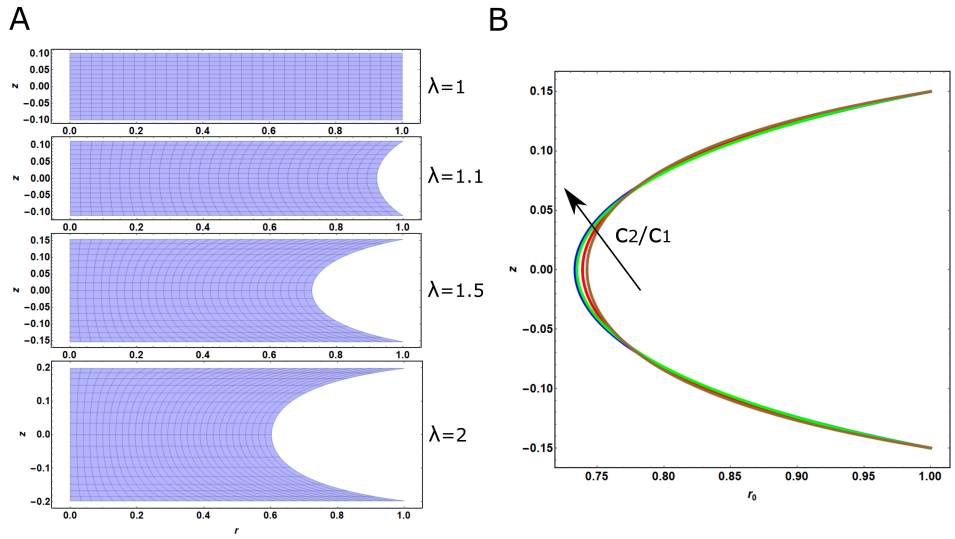

FIG. 2. (A) *Half-section of a deformed disc with initial aspect ratio* $R_0 = 10, L = 1$*, showing the axis-symmetric solution for* $c_2 = c_1$ *at different values axial stretch* λ*.* (B) *Comparison of the profile of the outer meniscus for an applied stretch* $\lambda = 1.5$ *at values of the stiffness ratio* $c_2/c_1 = 0$ *(brown),* 0.1 *(red),* 1 *(green), and* $c_1 = 0$ *(blue).*

3.2. Analytic solution for the extreme Mooney model ($c_1 = 0$). Equation 3.3 can also be integrated explicitly for an extreme Mooney strain energy density, such that

$$f = \sqrt{1 - A^2L^2}\sqrt{1 + \frac{(AZ)^2}{1 - A^2L^2}}, \qquad g = \frac{1}{A\sqrt{(1 - A^2L^2)}} \tan^{-1} \frac{AZ}{\sqrt{1 - A^2L^2}} \tag{3.9}$$

with

$$\lambda = \frac{\cos^{-1}\sqrt{1 - A^2L^2}}{AL\sqrt{1 - A^2L^2}}. \tag{3.10}$$

The analytic expressions (3.7) and (3.9) will be used in the following to derive explicit bifurcation conditions for both constitutive responses.

4. Linear bifurcation analysis. In this section we perform the linear stability analysis of the axis-symmetric solution given by (3.1), (3.5). First, we derive the incremental boundary value problem superposing an infinitesimal displacement over the finite strain. Second, we give the analytic solutions for the neo-Hookean and extreme Mooney cases. Finally, we introduce a suitable transformation of the general boundary value problem into a more convenient form, which is used to derive the numerical solution at varying physical ratio c_2/c_1.

4.1. Incremental boundary value problem. We superpose an incremental deformation vector $\delta\mathbf{x} = [u = u(R, \Theta, Z), v = v(R, \Theta, Z), w = w(R, \Theta, Z)]^T$ on the axis-symmetric stretched configuration [23]. In order to build a uniform asymptotic expansion we impose that $|\delta\mathbf{x}| << \min[R(f(0) - 1), L(\lambda - 1)]$. Accordingly, the ma-

terial gradient $\mathbf{\Gamma}$ of the incremental displacement reads

$$\mathbf{\Gamma} = \mathrm{Grad}(\delta\mathbf{x}) = \begin{bmatrix} u_{,R} & \frac{u_{,\Theta}-v}{R} & u_{,Z} \\ v_{,R} & \frac{v_{,\Theta}+u}{R} & v_{,Z} \\ w_{,R} & \frac{w,\Theta}{R} & w_{,Z} \end{bmatrix}, \tag{4.1}$$

where a comma indicates the partial derivative. With the aim to characterize the onset of a fingering instability centered at the disc midplane, the Dirichlet boundary conditions in (2.4) impose that $w(Z=0) = w(Z=\pm L) = 0$, while the assumption that the planes initially at constant Z remain planes in the deformed state imposes $w_{,R} = w_{,\Theta} = 0$. In the limit $L/R_0 << 1$ of thick cylinders, we can use a lubrication approximation with $w \ll u, v$, and $w_{,Z} \sim 0$. Accordingly, the incompressibility constraint at the leading incremental order is given by

$$\mathrm{tr}\mathsf{F}^{-1}\mathbf{\Gamma} = f^{-1}(Z)\left(u_{,R} + \frac{v_{,\Theta}+u}{R}\right) = 0. \tag{4.2}$$

By standard series expansions around the axis-symmetric solution, the components $\delta\mathbf{P}$ of the incremental nominal stress tensor read

$$\delta P_{ji} = A_{jikl}\Gamma_{lk} + p(R,Z)(F^{-1}\mathbf{\Gamma}F^{-1})_{ji} - \delta p\, F^{-1}_{ji} \quad \text{with} \quad (i,j,k,l) = (R,\Theta,Z), \tag{4.3}$$

where $\delta p = \delta p(R,\Theta,Z)$ is the increment of the Lagrange multiplier and $A_{jikl} = \frac{\partial^2\psi}{\partial F_{ij}\partial F_{lk}}$ are the elastic moduli evaluated in the deformed axis-symmetric configuration.

The bulk equilibrium equations for the boundary value problem at the leading incremental order read

$$\mathrm{Div}\delta\mathbf{P} = \mathbf{0}. \tag{4.4}$$

As for the axis-symmetric solution, we assume here that the boundary conditions at the deformed Neumann boundary are imposed only at the disc midplane, so that

$$\delta P_{RR} = \delta P_{R\Theta} = \delta P_{RZ} = 0 \qquad \text{at} \quad R = R_0, Z = 0, \tag{4.5}$$

where the last equality is automatically fulfilled by symmetry. Since the perturbed domain refers to a full cylinder, the displacement and stress components solving the boundary value problem must be bounded at $R = 0$ for the sake of physical compatibility. The solution of the incremental problem is sought by variable separation using the following ansatz:

$$\begin{cases} u(R,\Theta,Z) = (1-(f(Z))U(R)\cos(m\Theta), \\ v(R,\Theta,Z) = (1-(f(Z))V(R)\sin(m\Theta), \end{cases} \tag{4.6}$$

where m is an integer value representing the circumferential wavenumber of the fingering perturbation. For physical consistency, the stress components $\delta P_{RR}, \delta P_{R\Theta}, \delta P_{RZ}$ and the increment δp of Lagrange multiplier at the disc midplane read

$$\begin{cases} \delta P_{RR}(R,\Theta,Z=0) = S_{RR}(R)\cos(m\Theta), \\ \delta P_{R\Theta}(R,\Theta,Z=0) = S_{R\Theta}(R)\sin(m\Theta), \\ \delta P_{RZ}(R,\Theta,Z=0) = S_{RZ}(R)\cos(m\Theta), \\ \delta p(R,\Theta,Z=0) = Q(R)\cos(m\Theta). \end{cases} \tag{4.7}$$

Using the mirror symmetry over the midplane $Z = 0$, the incremental bulk equations given by (4.4) can be recast as a first-order ordinary differential system, known as Stroh formalism [33]:

$$\frac{d\boldsymbol{\eta}}{dR} = \frac{1}{R}\mathbf{G}\boldsymbol{\eta} = \frac{1}{R}\begin{bmatrix} \mathbf{G}_1 & \mathbf{G}_2 \\ \mathbf{G}_3 & \mathbf{G}_4 \end{bmatrix}\boldsymbol{\eta}, \tag{4.8}$$

where $\boldsymbol{\eta} = [U, V, R\ S_{RR}, R\ S_{R\Theta}]^T$ is the displacement-traction vector, and $\mathbf{G}$ is the so-called Stroh matrix. Using (4.2), (4.3), (4.6), (4.7), after some manipulation $\mathbf{G}$ can be decomposed into four 2×2 subblocks $\mathbf{G}_1$, $\mathbf{G}_2$, $\mathbf{G}_3$, $\mathbf{G}_4$ whose expressions are given in Appendix A. We finally remark that this generalized Stroh matrix is the pull-back of the one used in the classical Stroh formalism; therefore the four blocks do not display here the main symmetries of an Hamiltonian structure [22].

The differential system given by (4.8) must be solved with boundary conditions given by (4.5), substituting the axis-symmetric deformation field solving (3.3), (3.4) and the corresponding pressure field given by (3.5). We investigate the analytic solutions in the two cases of neo-Hookean and extreme Mooney models in the following.

4.2. Analytic solutions. We have derived in the previous section the analytic expressions of the axis-symmetric solutions of (3.3), (3.4) for neo-Hookean and extreme Mooney models, which will now be used to solve the incremental boundary value problem given by (4.8), (4.5)

4.2.1. Linear bifurcation of the neo-Hookean model. The analytic solution of the incremental problem for the neo-Hookean case in traction was given in [18]. Setting $c_2 = 0$, the differential system in (4.8) can be transformed into a fourth-order ordinary differential equation for $U(R)$, as follows:

$$\begin{aligned}
&\left(m^2-1\right)U(R)\left((f(0)-1)R^2p_{,RR}+2c_1f(0)^2\left((f(0)-1)\left(m^2-1\right)-R^2f''(0)\right)\right)\\
&+RU'(R)\left(2c_1f(0)^2\left(3R^2f''(0)-(f(0)-1)\left(2m^2+1\right)\right)-(f(0)-1)R\left(2p_{,R}+Rp_{,RR}\right)\right)\\
&+R^3\left((1-f(0))p_{,R}+2c_1f(0)^2\left(R^2f''(0)-(f(0)-1)\left(2m^2-5\right)\right)\right)U''(R)\\
&+(12c_1(f(0)-1)f(0)^2R^3)U'''(R)+(2c_1(f(0)-1)f(0)^2R^4)U''''(R)=0,
\end{aligned} \tag{4.9}$$

where $p_{,RR} = p_{,RR}(R, 0)$, $p_{,R} = p_{,R}(R, 0)$. Using the basic solution in (3.5), (3.7), (3.8) and avoiding singularities at $R = 0$, the general bounded solution of (4.9) reads

$$U(R) = d_1\left(\frac{R}{R_0}\right)^{m-1} + d_2\frac{I_m(AR/\sqrt{1-f(0)})}{RI_m(AR_0/\sqrt{1-f(0)})}, \tag{4.10}$$

where d_1, d_2 are two arbitrary constants, I_m is the modified Bessel function of the first kind of order m, and $A = A(\lambda)$ is given by (3.8). Moreover, the boundary conditions at $R = R_0$ in (3.4) can be simplified as

$$\begin{cases}
p(R_0,0)\left(\left(m^2-1\right)U(R)-R_0U'(R)\right)+2c_1f(0)^2R_0\left(R_0U''(R)+2U'(R)\right)=0;\\
U(R)\left(-(f(0)-1)\left(m^2-1\right)R_0p_{,R}(R_0,0)-2c_1f(0)^2\left(R_0^2f''(0)+(f(0)-1)\left(m^2-1\right)\right)\right)\\
+R_0U'(R)\big((f(0)-1)(m^2p(R_0,0)+R_0p_{,R}(R,0))\\
\qquad\qquad+2c_1f(0)^2\left((f(0)-1)\left(2m^2-1\right)-R_0^2f''(0)\right)\big)\\
-2c_1(f(0)-1)f(0)^2R_0^2\left(R_0U'''(R)+4U''(R)\right)=0.
\end{cases} \tag{4.11}$$

Substituting (4.10) in (4.11), the boundary conditions can be rewritten as $\mathbf{M}.\mathbf{d} = 0$, where $\mathbf{d} = [d_1, d_2]^T$ and $\mathbf{M}$ is a 2×2 matrix. Accordingly, the dispersion relation

$\det \mathbf{M} = 0$ relates the stretch threshold λ at which the perturbation with wavenumber m become marginally stable. The critical value λ_{cr} can be computed as the lowest stretch at which a critical mode m_{cr} appears. The corresponding marginally stable curves become degenerate as $L/R_0 \to 0$ since we find that $m_{cr} \to \infty$ and $\lambda_{cr} \to 1$. This degeneracy highlights an ill-posedness of the neo-Hookean model, which becomes always unstable with respect to any infinitesimal displacement, developing arbitrary small fingering perturbations.

4.2.2. Linear bifurcation of the extreme Mooney model. The analytic solution of the extreme Mooney case is given here for the first time. Setting $c_1 = 0$, we find from (3.3) that $f''(0) = A^2/f(0)$ and from (3.6) that

$$B = f(0)^2 \left(A^2 R_0^2 - 2f(0)^2\right)/2.$$

Accordingly, the differential system in (4.8) simplifies the following fourth-order ordinary differential equation for $U(R)$:

(4.12)
$$\begin{aligned}
&\left(m^2-1\right)\left(-A^2 f(0)^5 R^2 + (f(0)-1)m^2 - f(0) + 1\right) U(R) \\
&+ R\left((f(0)-1)m^2\left(A^2 f(0)^4 R^2 - 2\right) - f(0)\left(A^2(f(0)-4)f(0)^3 R^2 + 1\right) + 1\right) U'(R) \\
&+ R^2 U''(R)\left(A^2(5-4f(0))f(0)^4 R^2 - 2(f(0)-1)m^2 + 5(f(0)-1)\right) \\
&+ (f(0)-1)R^3\left(U'''(R)\left(6 - A^2 f(0)^4 R^2\right) + R U''''(R)\right) = 0,
\end{aligned}$$

where $A = A(\lambda)$ is given by (3.10). The bounded general solution of (4.12) reads

$$U(R) = d_1 \left(\frac{R}{R_0}\right)^{m-1} + d_2 \left(\frac{R}{R_0}\right)^{m-1} \frac{{}_1F_1\left(\delta_1, m+1, \frac{1}{2}A^2 f(0)^4 R^2\right)}{{}_1F_1\left(\delta_1, m+1, \delta_2\right)}, \tag{4.13}$$

where d_1, d_2 are two arbitrary constants, and ${}_1F_1$ denotes the generalized hypergeometric function [14], and

$$\delta_1 = \frac{1}{2}\left(\frac{1}{1-f(0)} + m - 2\right);\ \delta_2 = \frac{1}{2}A^2 f(0)^4 R_0^2.$$

Moreover, the boundary conditions at $R = R_0$ in (3.4) can be simplified as

$$\begin{cases}
\left(m^2-1\right)U(R) + R_0\left(R_0 U''(R) + U'(R)\right) = 0; \\
-2\left(A^2 f(0)^5 R_0^2 + (f(0)-1)m^2 - f(0) + 1\right) U(R) \\
+ R_0 U'(R)\left(2A^2(f(0)-2)f(0)^4 R_0^2 + 6(f(0)-1)m^2 - 2f(0) + 2\right) \\
+ 2(f(0)-1)R_0^2\left(\left(A^2 f(0)^4 R_0^2 - 4\right)U''(R) - R_0 U'''(R)\right) = 0.
\end{cases} \tag{4.14}$$

Substituting (4.13) in (4.14), the boundary conditions can be recast as $\mathbf{M}.\mathbf{d} = 0$. Recalling that $A = \frac{\sqrt{1-f(0)}}{L}$ from (3.9), the dispersion relation $\det \mathbf{M} = 0$ reads

$$\gamma_1\ {}_1F_1\left(\delta_1, m+2, \delta_2\right) + \gamma_2\ {}_1F_1\left(\delta_1, m+3, \delta_2\right) = 0 \tag{4.15}$$

with

$$\begin{aligned}
\gamma_1 &= 4f(0)^4 L^2 m R_0^2(-2(f(0)-1)m + 3f(0) - 2) \\
&\quad + 2(f(0)-1)f(0)^8 R_0^4(f(0)(m-2) - m + 1) + 8L^4 m\left(m^2-1\right); \\
\gamma_2 &= f(0)^4 R_0^2(f(0)(m+4) - m - 3)\left(f(0)^4 R_0^2(f(0)(m-2) - m + 1) - 4L^2(m-1)m\right).
\end{aligned}$$

Notably, we find that (4.15) cannot be fulfilled for any $m, f(0) < 1$, meaning that a cylinder made by an extreme Mooney solution does not undergo a fingering instability and remain axis-symmetric for any applied stretch $\lambda > 1$. This is in accordance with what was observed in [19] for rubber cylinders under tensile traction, suggesting that the physical nonlinearity given by $c_2 > 0$ may stabilize against the onset of fingering. In the following, we propose a numerical procedure to solve the incremental boundary value problem for a generic Mooney–Rivlin material, with the aim to investigate how geometric and physical nonlinearities affect the emergence of such a fingering instability.

4.3. Linear bifurcation for the Mooney–Rivlin model: Numerical procedure. For a generic Mooney–Rivlin material, the axis-symmetric solution is given in terms of elliptic integrals and it is not possible to solve analytically the incremental boundary value problem given by (4.8), (4.5). In the following, we propose a robust numerical procedure based on employing the impedance matrix method for solving the incremental elastic problem [32]. In particular, let us define the 4×4 matricant $\mathbf{T}(R, R_i)$ as the solution of the initial value problem:

$$\left(\frac{d}{dR} - \frac{1}{R}\mathbf{G}\right)\mathbf{T}(R, R_i) = \mathbf{0} \qquad \text{with} \quad \mathbf{T}(R_i, R_i) = \mathbf{I}_{(4)}, \quad R, R_i \neq 0, \tag{4.16}$$

where $\mathbf{I}_{(4)}$ is the 4×4 identity matrix. Thus, from (4.8) and (4.16), the solution $\boldsymbol{\eta}$ can be expressed as follows:

$$\boldsymbol{\eta}(R) = \mathbf{T}(R, R_i)\boldsymbol{\eta}(R_i) = \begin{bmatrix} \mathbf{T}_1(R, R_i) & \mathbf{T}_2(R, R_i) \\ \mathbf{T}_3(R, R_i) & \mathbf{T}_4(R, R_i) \end{bmatrix} \boldsymbol{\eta}(R_i), \tag{4.17}$$

where $\mathbf{T}(R, R_i)$ is the *matricant* for a generic $R_i \neq 0$, such that $\mathbf{T}(R_i, R_i) = \mathbf{I}_{(4)}$, and $\mathbf{T}_j$, $j = (1, 2, 3, 4)$ are its four 2×2 subblocks.

The incremental displacement $\mathbf{u}$ and traction $\mathbf{S}$ vectors read

$$\mathbf{u} = [U(R), V(R)]^T; \qquad \mathbf{S} = [S_{RR}(R), S_{R\Theta}(R)]^T \tag{4.18}$$

so that $\boldsymbol{\eta} = [\mathbf{u}, R\mathbf{S}]^T$. From (4.17), we are allowed to define the following relation between the traction and the displacements vectors:

$$R\mathbf{S} = \mathbf{Z}\ \mathbf{u}, \tag{4.19}$$

where $\mathbf{Z} = \mathbf{Z}(R, R_i) = \mathbf{T}_3(R, R_i)\mathbf{T}_1^{-1}(R, R_i)$ is the *conditional* (i.e., depending on its value at $R = R_i$) impedance matrix.

By substituting (4.19) and eliminating the dependence on $\mathbf{u}$, (4.8) can be transformed into a Riccati differential equation for $\mathbf{Z}$ [9], reading

$$\frac{d\mathbf{Z}}{dR} = \frac{1}{R}\left(\mathbf{G}_3 + \mathbf{G}_4\mathbf{Z} - \mathbf{Z}\mathbf{G}_2\mathbf{Z} - \mathbf{Z}\mathbf{G}_1\right). \tag{4.20}$$

Since (4.17) has a regular singular point for $R_i = 0$, the matricant solution of a solid cylinder can be sought in the form of a Frobenius series [32]. Let the *central-impedance matrix* $\mathbf{Z}_0$ be the solution of the right-hand side of (4.19) computed at $R = 0$. Considering the Taylor expansion $\mathbf{Z}(R) \sim \mathbf{Z}_0 + R^2\mathbf{Z}_1 + o(R^2)$, the matrix $\mathbf{Z}_1$ can be calculated from (4.20) at the second order in R. Using a starting point $0 < R_i \ll R_0$, we numerically integrate $\mathbf{Z}(R)$ in (4.20) from the initial value $\mathbf{Z}(R_i) = \mathbf{Z}_0 + R_i^2\mathbf{Z}_1$, where $\mathbf{Z}_0$ and $\mathbf{Z}_1$ are the leading-order stable solutions for $R = R_i$ [7].

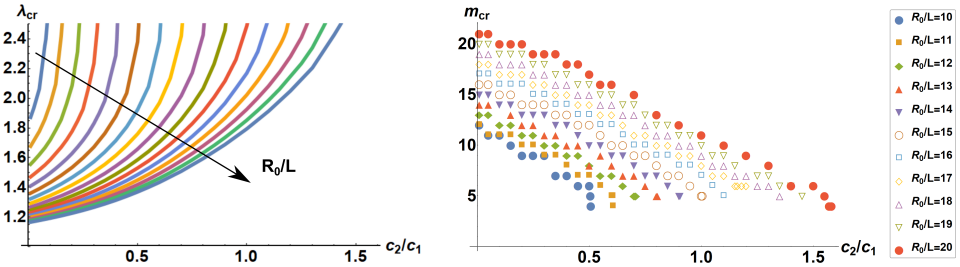

FIG. 3. *Marginal stability curves of elastic fingering for the Mooney–Rivlin strain energy in* (2.1). *Left: Critical value* λ_{cr} *of the axial stretch versus the stiffness ratio* c_2/c_1 *at different values of the initial aspect ratio* R_0/L, *shown at unit steps from* 5 *to* 20. *Right: Critical wavenumber* m_{cr} *for fingering versus the stiffness ratio* c_2/c_1 *at different initial aspect ratios* R_0/L.

Accordingly, the Neumann boundary conditions in (4.5) can be recast as

$$\det \mathbf{Z}(R_o) = \mathbf{0}, \tag{4.21}$$

which is used as the stop condition of the numerical procedure, while performing iterations on all the geometric and physical coefficients of the incremental elastic problem. These numerical results are summarized in the next section.

5. Results. In this section, we first discuss the marginal stability results for the onset of elastic fingering in a generic Mooney–Rivlin material as a function of the aspect ratio L/R_0 and the physical ratio c_2/c_1. Second, we study the nonlinear pattern formation by means of mixed finite-element computations.

5.1. Marginal stability thresholds. The marginal stability thresholds for the Mooney–Rivlin strain energy in (2.1) have been computed by numerical integration of (4.20) with initial values set at $R_i = R_0/100$, performing iterations on the physical and geometrical parameters until the stop condition given by (4.21) is reached. In Figure 3 we depict the critical values of the axial stretch λ_{cr} (left) and the wavenumber m_{cr} (right) versus the stiffness ratio c_2/c_1 at different values of the initial aspect ratio R_0/L. At fixed stiffness ratio c_2/c_1, we remark that the effect of geometric nonlinearity obtained by increasing the initial aspect ratio R_0/L favors the onset of elastic fingering. We find that the critical stretch decreases by increasing R_0/L, while the corresponding fingering occurs at shorter length-scales since m also increases. In Figure 4 we also depict the critical values of the axial stretch λ_{cr} (left) and the wavenumber m_{cr} (right) versus the initial aspect ratio L/R_0 at different values of the stiffness ratio c_2/c_1. Physical nonlinearity is investigated by varying the stiffness ratio c_2/c_1 at fixed initial aspect ratio R_0/L, and they are found to have a stabilizing effect versus fingering.

In fact, the critical axial stretch increases by increasing the ratio c_2/c_1 at fixed initial geometry, while the typical fingering length-scale also increases. In this sense, we prove that the presence of constitutive nonlinearities regularizes the unphysical short-wavelength fingering that was earlier discussed in the neo-Hookean limit for stubby cylinders. Furthermore, the curves for the critical stretch in Figures 3 and 4 (left) display a vertical asymptote at a limiting value of c_2/c_1 that increases by increasing the initial aspect ratio R_0/L. In physical terms, this means that at this limiting value of c_2/c_1, physical nonlinearities dominate geometric nonlinearities, and elastic fingering is completely suppressed. This is in accordance with previous experimental and numerical results on hydrogels and rubberlike materials [19, 12].

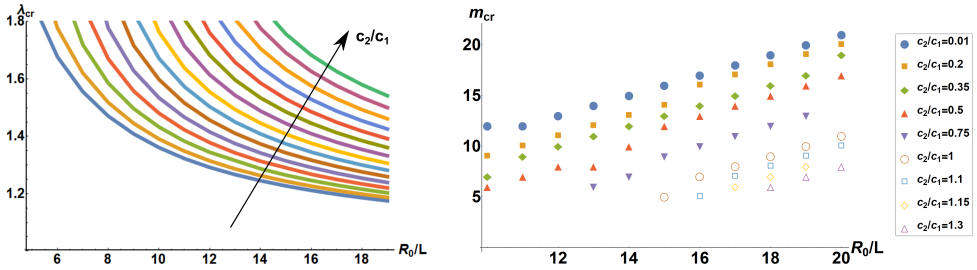

FIG. 4. *Marginal stability curves of elastic fingering for the Mooney–Rivlin strain energy in* (2.1). *Left: Critical value* λ_{cr} *of the axial stretch versus the initial aspect ratios* R_0/L *at different values of the stiffness ratio* c_2/c_1, *shown in a range from* 0.01 *to* 1.5. *Right: Critical wavenumber* m_{cr} *for fingering versus the initial aspect ratios* R_0/L *at different values of the stiffness ratio* c_2/c_1.

In the following we investigate the fully developed nonlinear elastic fingering using finite element simulations.

5.2. Finite element simulations. A finite element model of the nonlinear elastic problem is implemented in the commercial software ABAQUS 6.14 (Dassault Systémes Simulia Corporation, Johnston, RI). A mixed formulation is implemented to avoid numerical difficulties related to the co-existence of multiple bifurcation paths in nearly incompressible models, using high-order elements in the displacements to avoid numerical locking [10]. In particular, the three-dimensional geometry is discretized by using a mesh of 10-node modified quadratic tetrahedron, hybrid with linear pressure (C3D10MH); the total number of elements in each simulation is a consequence of the choice to have 20 elements through the thickness and to discretize the lateral surface in such a way that there are 10 elements for each wavelength, when considering the mode m_{cr} predicted by the theoretical analysis for the specific set of geometrical and constitutive parameters. We used an implicit solver and a static procedure without any stabilization enforced. These features are sufficient to provide a high-resolution description of the fingering pattern but would require more sophisticated continuation algorithms and parallelization techniques to investigate the nonlinear pattern development in the postbifurcation regime [26, 12]. The numerical analysis of the elastic fingering is performed varying separately the aspect ratio R_0/L of the cylinder at fixed stiffness ratio c_2/c_1 and vice versa. Since we used a static analysis without any numerical stabilization, we facilitate the emergence of the pattern by perturbing sinusoidally the outer radius of the underformed cylinder as $R(Z) = R_0 + A_0\left(Z^2/L^2 - 1\right)\cos m_{cr}\Theta$, so that it decays parabolically from the midsection of the cylinder toward the ends. We set $A_0 = 0.002R_0$ and m_{cr} is the critical wavenumber predicted by the linear bifurcation analysis. Dirichlet boundary conditions are applied to the bases: the in-plane displacement is fixed to zero, while the cylinder is stretched by imposing the displacement of all the points of the bases along the z-direction.

An illustrative sketch of the simulation results is given in Figure 5, where we compare the deformed shapes of the meniscus for a disc with initial shape ratio $R_0/L = 10$ and two different values of the stiffness ratio c_2/c_1 at the displayed increasing values of the applied stretch λ. For $c_2/c_1 = 0.4$ the disc develops a fingering morphology at the critical thresholds predicted by the linear bifurcation analysis, while for $c_2/c_1 = 0.7$ the meniscus keeps the axis-symmetric shape given by the ground state.

We study the fingering morphology by computing the evolution of the amplitude $A = (\max|r(R_0, Z = 0)| - \min|r(R_0, Z = 0)|)/2$ of the emerging pattern at the

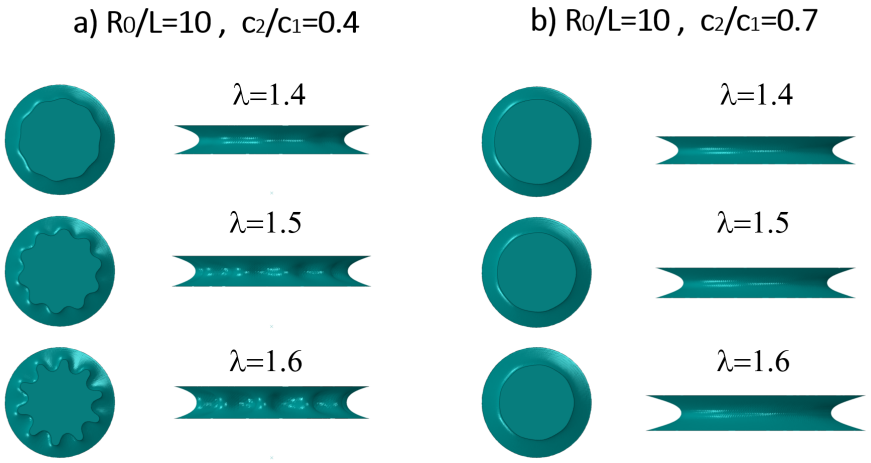

FIG. 5. *Simulation results of the deformed shapes and midsections of a bonded disc with initial shape ratio* $R_0/L = 10$ *at applied stretch* $\lambda = 1.4, 1.5, 1.6$*, shown for* (a) $c_2/c_1 = 0.4$ *(left) and* (b) $c_2/c_1 = 0.7$ *(right).*

midplane of the cylinder. We found that the presence of an initial imperfection results in a slight anticipation of the critical stretch threshold in simulations, which is marked by a sudden increase of A over the applied stretch λ. The presence of a continuous morphological transition that is completely reversed after unloading highlights that the bifurcation is supercritical.

We first turn our attention to the effect of the geometric nonlinearity on the emerging fingering pattern. Thus, we vary the aspect ratio R_0/L of the cylinder at fixed stiffness ratio $c_2/c_1 = 0.3$. The range of variation of R_0/L is set between 10 and 20, since for more slender cylinders our lubrication approximation would fail and fringe modes might prevail [17]. Figure 6(a) shows the resulting evolution of the amplitude A in response to the increasing applied stretch λ for five values of initial aspect ratio. In agreement with the linear bifurcation analysis, we find that the critical stretch threshold decreases while increasing the ratio R_0/L. Moreover, the increase of A in the weakly nonlinear regime of patterning is dependent on the aspect ratio, showing a more marked topological transition toward narrow fingers as R_0/L decreases, i.e., in a regime where geometrical nonlinearities become more relevant.

Second, we investigated the effect of physical nonlinearity by varying the stiffness ratio c_2/c_1 at fixed the aspect ratio $R_0/L = 10$ of the cylinder. In Figure 7 we plot the amplitude A of the pattern over the applied stretch λ, recovering the stabilizing effect of increasing c_2/c_1 on the linear bifurcation threshold for the stretch, up to the limit beyond which fingering is completely suppressed. We also find that physical nonlinearity has a marked effect on the nonlinear morphology of the pattern, with a crossover from rounded to starred fingering as c_2/c_1 increases. This is also depicted by the four snapshots of the deformed bifurcated morphology at different values of c_2/c_1.

6. Discussion and conclusions. This work provides fundamental understanding of elastic fingering in soft isotropic cylinders under traction. Recent experiments have shown that the onset of such an elastic bifurcation is driven by a complex interplay of nonlinearities in the hyperelastic functional, which is subjected to the

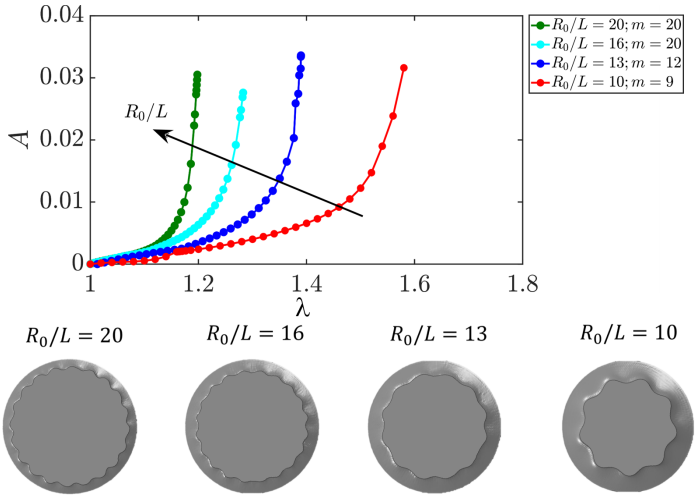

FIG. 6. *Finite element simulations of a disc with* $c_2/c_1 = 0.3$ *showing (top) the simulated fingering amplitude* A *versus the applied stretch* λ *and (bottom) the midsections at different values of the initial aspect ratio* R_0/L.

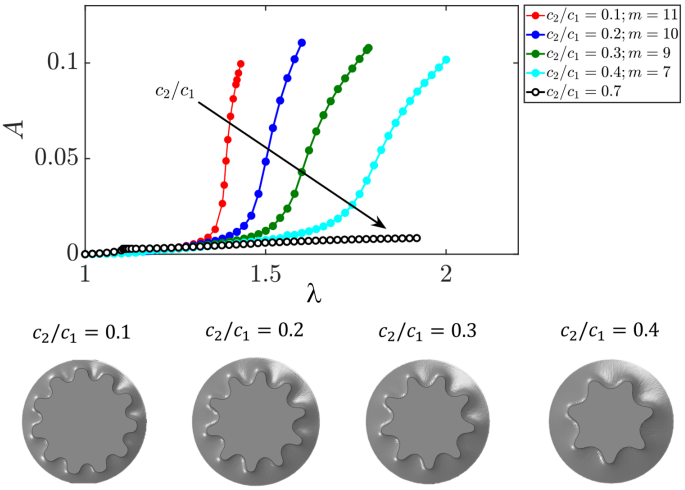

FIG. 7. *Finite element simulations of a disc with* $R_0/L = 10$ *showing (top) the simulated fingering amplitude* A *versus the applied stretch* λ *and (bottom) the midsections at different values of the stiffness ratio* c_2/c_1. *For* $c_2/c_1 > 0.5$ *fingering is suppressed, in accordance with the theoretical predictions of Figure* 3.

nonconvex incompressibility constraint. The elastic boundary value problem for a Mooney–Rivlin material is indeed characterized by two dimensionless parameters, the initial aspect ratio R_0/L and the stiffness ratio c_2/c_1, that are related to geometric and physical nonlinearities, respectively. The rigid constraints at the end bases impose the formation of an axis-symmetric meniscus after the application of a finite axial displacement. The shape of such a meniscus can be given in the form of an elliptic integral, becoming deeper as the stiffness ratio increases as shown in Figure 2. We characterized the bifurcation from this ground state to a fingering morphology making a lubrication approximation, which allows us to rewrite the incremental boundary value problem

for a variable separation ansatz in the form of a generalized Stroh formalism, as in (4.8). First, analytic solutions for the neo-Hookean ($c_2 = 0$) and extreme Mooney ($c_1 = 0$) materials are given, as in (4.10) and (4.13), respectively. The neo-Hookean model only accounts for geometric nonlinearity and shows that the critical stretch threshold decreases as R_0/L increases. Nonetheless, this particular model becomes ill-posed for such thin geometry, since the critical circumferential wavelength also goes to zero, highlighting a violation of the complementing condition at the free boundary [1]. Conversely, we find that elastic fingering is completely suppressed for the extreme Mooney materials. In this case, physical nonlinearity counteracts the destabilizing geometric effect. In this sense, elastic fingering of soft cylinders resembles the bulging of elastic tubes under pressure [8, 25]. Second, we used the impedance matrix method to rewrite the incremental boundary problem in the form of a Riccati differential equation, as in (4.20), that is solved using a robust numerical procedure. The results depicted in Figures 3 and 4 prove that an increase of the stiffness ratio c_2/c_1 provokes an increase of both the critical stretch threshold and the pattern wavelength, up to a critical asymptotic value where fingering is suppressed. Such a limiting value is controlled by the initial aspect ratio of the cylinder, confirming the regularizing effect of physical nonlinearity on the bifurcation thresholds observed in experiments. Finally, we performed numerical simulations of the hyperelastic problem using a mixed finite element formulation, whose results are depicted in Figures 6 and 7. We find that the postbifurcation morphology of the developing fingers is also smoothed by the physical nonlinearity. While the bifurcation is always a supercritical pitchfork, the amplitude of the bifurcated branch becomes smaller as c_2/c_1 increases, up to the complete suppression of the fingering. The morphology of the fingers displays a crossover from rounder to starred shapes as the physical nonlinearity is increased.

In conclusion, our theoretical and numerical results have uncovered the mathematical nature of fingering in soft cylinders. Such an elastic instability is very different from viscous fingering in fluid-fluid interfaces. The bifurcation of the confined elastic meniscus to a fingered shape is enabled by large displacements controlling the strain localization at the free boundary. Interestingly, a higher negative Gaussian curvature of the meniscus is found to favor such an elastic fingering, while a curvature-induced rigidity effect is known to prevent buckling of elastic shells [34]. This is because a topological transition breaking the axial symmetry can be accommodated in the bulk at a lower global energetic cost due to geometric nonlinearity in the energy functional. Nonetheless, the physical nonlinearity that is encoded in the linear dependence on I_2 of the elastic energy is found to exert an opposite stabilizing effect: the additional energy dependence on I_2 penalizes the local surface stretching at the free boundary that would arise as a consequence of the Gauss' egregium theorem. The new insights on the interplay of physical and geometrical nonlinearities beneath fingering instability in soft elastic cylinders are finally important for several applications, such as the design of smart actuators or soft adhesive joints.

Appendix A. Subblocks of the Stroh matrix. The subblocks of the Stroh matrix in (4.8) read

$$\mathbf{G}_1 = \begin{bmatrix} -1 & m \\ \frac{f(0)^2 m\left(p(R,0)-2c_2 f(0)^4\right)}{2(c_1 f(0)^4+c_2)} & \frac{f(0)^2 p(R,0)-2c_2 f(0)^6}{2(c_1 f(0)^4+c_2)} \end{bmatrix};$$

$$\mathbf{G}_2 = \begin{bmatrix} 0 & 0 \\ 0 & \frac{f(0)^4}{2(f(0)-1)(c_1 f(0)^4+c_2)} \end{bmatrix};$$

$$\text{(A.1)}\quad \mathbf{G}_4 = \begin{bmatrix} 1 & \frac{f(0)^2 m\left(2c_2 f(0)^4 - p(R,0)\right)}{2(c_1 f(0)^4 + c_2)} \\ m & \frac{2c_2 f(0)^5\left(R^2 f''(0) + f(0)\right) - f(0)^2 p(R,0)}{2(c_1 f(0)^4 + c_2)} \end{bmatrix}; \qquad \mathbf{G}_3 = \begin{bmatrix} \gamma_{11} & \gamma_{12} \\ \gamma_{21} & \gamma_{22} \end{bmatrix};$$

with

$$\begin{aligned}
\gamma_{11} &= \frac{2(f(0)-1)\left(c_2\left(f(0)^6-1\right)-c_1 f(0)^4\right)\left(c_1 f(0)^4\left(m^2+2\right)+c_2\left(\left(f(0)^6+1\right)m^2+2\right)\right)}{f(0)^4(c_1 f(0)^4+c_2)},\\
\gamma_{12} &= \frac{(f(0)-1)p(R,0)\left(4\left(c_1 f(0)^4+c_2 f(0)^6 m^2+c_2\right)-f(0)^2 m^2 p(R,0)\right)}{2f(0)^2(c_1 f(0)^4+c_2)} - 2R^2 f''(0)(c_1+c_2 f(0)(3f(0)-2)),\\
\gamma_{21} &= \frac{(f(0)-1)m\left(4f(0)^2 p(R,0)\left(c_1 f(0)^4+c_2 f(0)^6+c_2\right)-f(0)^4 p(R,0)^2-8c_2 f(0)^5 R^2 f''(0)\left(c_1 f(0)^4+c_2\right)\right)}{2f(0)^4(c_1 f(0)^4+c_2)}\\
&\quad + \frac{2(f(0)-1)m\left(c_1 f(0)^4-c_2 f(0)^6+c_2\right)\left(3c_1 f(0)^4+c_2\left(f(0)^6+3\right)\right)}{f(0)^4(c_1 f(0)^4+c_2)},\\
\gamma_{22} &= \frac{-2f(0)^4 R^2 f''(0)\left(2\left(c_1^2 f(0)^4+c_1 c_2\left((2f(0)-1)f(0)^5+1\right)+c_2^2\left(f(0)^7-f(0)^6+2f(0)-1\right)f(0)\right)\right)}{2f(0)^4(c_1 f(0)^4+c_2)}\\
&\quad + \frac{2f(0)^4 R^2 f''(0)\left(c_2(f(0)-1)f(0)^3 p(R,0)\right)}{2f(0)^4(c_1 f(0)^4+c_2)}\\
&\quad + \frac{(f(0)-1)f(0)^2 p(R,0)\left(-f(0)^2 p(R,0)+4c_1 f(0)^4 m^2+4c_2\left(f(0)^6+m^2\right)\right)}{2f(0)^4(c_1 f(0)^4+c_2)}\\
&\quad - \frac{4(f(0)-1)\left(c_2\left(f(0)^6-1\right)-c_1 f(0)^4\right)\left(c_1 f(0)^4\left(2m^2+1\right)+c_2\left(f(0)^6+2m^2+1\right)\right)}{2f(0)^4(c_1 f(0)^4+c_2)}.
\end{aligned}$$

Acknowledgments. P. Ciarletta and M. Taffetani are members of GNFM of the Istituto Nazionale di Alta Matematica (INdAM). The authors thank Shaoting Lin and Xuanhe Zhao for granting permission to reproduce the experimental images in Figure 1.

REFERENCES

[1] S. Agmon, A. Douglis, and L. Nirenberg, *Estimates near the boundary for solutions of elliptic partial differential equations satisfying general boundary conditions* II, Comm. Pure Appl. Math., 17 (1964), pp. 35–92.

[2] M. Ben Amar and D. Bonn, *Fingering instabilities in adhesive failure*, Phys. D, 209 (2005), pp. 1–16.

[3] E. Ben-Jacob, N. Goldenfeld, B. Kotliar, and J. Langer, *Pattern selection in dendritic solidification*, Phys. Rev. Lett., 53 (1984), pp. 2110–2113.

[4] D. Bensimon, L. P. Kadanoff, S. Liang, B. I. Shraiman, and C. Tang, *Viscous flows in two dimensions*, Rev. Modern Phys., 58 (1986), pp. 977–989.

[5] J. S. Biggins, B. Saintyves, Z. Wei, E. Bouchaud, and L. Mahadevan, *Digital instability of a confined elastic meniscus*, Proc. Natl. Acad. Sci., 110 (2013), pp. 12545–12548.

[6] J. S. Biggins, Z. Wei, and L. Mahadevan, *Fluid-driven fingering instability of a confined elastic meniscus*, Europhys. Lett., 110 (2015), 34001.

[7] P. Ciarletta and M. Destrade, *Torsion instability of soft solid cylinders*, IMA J. Appl. Math., 79 (2014), pp. 804–819.

[8] A. H. Corneliussen and R. Shield, *Finite deformation of elastic membranes with application to the stability of an inflated and extended tube*, Arch. Ration. Mech. Anal., 7 (1961), pp. 273–304.

[9] M. Destrade, A. N. Annaidh, and C. D. Coman, *Bending instabilities of soft biological tissues*, Int. J. Solids Structures, 46 (2009), pp. 4322–4330.

[10] P. Farrell and C. Maurini, *Linear and nonlinear solvers for variational phase-field models of brittle fracture*, Internat. J. Numer. Methods Engrg., 109 (2017), pp. rg–667.

[11] A. Ghatak and M. K. Chaudhury, *Adhesion-induced instability patterns in thin confined elastic film*, Langmuir, 19 (2003), pp. 2621–2631.

[12] B. Giovanardi, A. A. Śliwiak, A. Koshakji, S. Lin, X. Zhao, and R. Radovitzky, *A path-following simulation-based study of elastic instabilities in nearly-incompressible confined cylinders under tension*, J. Mech. Phys. Solids, 131 (2019), pp. 252–275.

[13] Y. Grabovsky and L. Truskinovsky, *Marginal material stability*, J. Nonlinear Sci., 23 (2013), pp. 891–969.

[14] I. S. Gradshteyn and I. M. Ryzhik, *Table of Integrals, Series, and Products*, Academic Press, New York, 2014.

[15] G. M. Homsy, *Viscous fingering in porous media*, Annu. Rev. Fluid Mech., 19 (1987), pp. 271–311.
[16] W. W. Klingbeil and R. T. Shield, *Large-deformation analyses of bonded elastic mounts*, Z. Angew. Math. Phys., 17 (1966), pp. 281–305.
[17] S. Lin, T. Cohen, T. Zhang, H. Yuk, R. Abeyaratne, and X. Zhao, *Fringe instability in constrained soft elastic layers*, Soft Matter, 12 (2016), pp. 8899–8906.
[18] S. Lin, Y. Mao, R. Radovitzky, and X. Zhao, *Instabilities in confined elastic layers under tension: Fringe, fingering and cavitation*, J. Mech. Phys. Solids, 106 (2017), pp. 229–256.
[19] S. Lin, Y. Mao, H. Yuk, and X. Zhao, *Material-stiffening suppresses elastic fingering and fringe instabilities*, Int. J. Solids Structures, 139 (2018), pp. 96–104.
[20] A. Lindner, D. Bonn, E. C. Poiré, M. B. Amar, and J. Meunier, *Viscous fingering in non-newtonian fluids*, J. Fluid Mech., 469 (2002), pp. 237–256.
[21] M. Mooney, *A theory of large elastic deformation*, J. Appl. Phys., 11 (1940), pp. 582–592.
[22] A. N. Norris and A. Shuvalov, *Elastodynamics of radially inhomogeneous spherically anisotropic elastic materials in the stroh formalism*, Proc. A, 468 (2011), pp. 467–484.
[23] R. W. Ogden, *Non-linear Elastic Deformations*, Courier Corporation, Chelmsford, MA, 1997.
[24] L. Paterson, *Radial fingering in a Hele Shaw cell*, J. Fluid Mech., 113 (1981), pp. 513–529.
[25] S. P. Pearce and Y. B. Fu, *Characterization and stability of localized bulging/necking in inflated membrane tubes*, IMA J. Appl. Math., 75 (2010), pp. 581–602.
[26] E. Riks, *An incremental approach to the solution of snapping and buckling problems*, Int. J. Solids Structures, 15 (1979), pp. 529–551.
[27] R. S. Rivlin, *Large elastic deformations of isotropic materials* IV. *Further developments of the general theory*, Philos. Trans. A, 241 (1948), pp. 379–397.
[28] P. Saffman, *Viscous fingering in Hele-Shaw cells*, J. Fluid Mech., 173 (1986), pp. 73–94.
[29] P. G. Saffman and G. I. Taylor, *The penetration of a fluid into a porous medium or Hele-Shaw cell containing a more viscous liquid*, Proc. A, 245 (1958), pp. 312–329.
[30] B. Saintyves, O. Dauchot, and E. Bouchaud, *Bulk elastic fingering instability in Hele-Shaw cells*, Phys. Rev. Lett., 111 (2013), 047801.
[31] K. R. Shull, C. M. Flanigan, and A. J. Crosby, *Fingering instabilities of confined elastic layers in tension*, Phys. Rev. Lett., 84 (2000), pp. 3057–3060.
[32] A. Shuvalov, *A sextic formalism for three-dimensional elastodynamics of cylindrically anisotropic radially inhomogeneous materials*, Proc. A, 459 (2003), pp. 1611–1639.
[33] A. Stroh, *Steady state problems in anisotropic elasticity*, J. Math. Phys., 41 (1962), pp. 77–103.
[34] M. Taffetani, F. Box, A. Neveu, and D. Vella, *Limitations of curvature-induced rigidity: How a curved strip buckles under gravity*, Europhys. Lett., 127 (2019), 14001.
[35] C. Truesdell and W. Noll, *The non-linear field theories of mechanics*, Handb. Phys., 2 (1965), pp. 1–541.